Exploring Mid-IR FSO Communications with Unipolar Quantum Optoelectronics

Mahdieh Joharifar, *Student Member, IEEE,* Hamza Dely, Laureline Durupt, Richard Schatz, Gregory Maisons, Djamal Gacemi, Armands Ostrovskis, Lu Zhang, Toms Salgals, Yan-Ting Sun, Sandis Spolitis, Vjačeslavs Bobrovs, Xianbin Yu, *Senior Member, IEEE,* Angela Vasanelli, Carlo Sirtori, Oskars Ozolins, *Senior Member, IEEE,* Xiaodan Pang, *Senior Member, IEEE*

***Abstract*— Free space optical (FSO) communication is considered a critical part of future ICT infrastructure, particularly in non-terrestrial communication segments. In this context, the ability to achieve fast and reliable FSO propagation through long-distance atmospheric channels is the most important factor in choosing technological solutions. One property of optics directly related to this factor is the choice of wavelength. It has been identified that the mid-infrared (mid-IR) regime, which includes two atmospheric transmission windows—the mid-wave IR (MWIR, 3-5 µm) and the long-wave IR (LWIR, 8-12 µm)—can potentially offer a promising solution for achieving such performance. Additionally, viable semiconductor sources and detectors that support high-speed and efficient signal transmission are also considered critical to generating sufficient critical mass to advance the application of mid-IR FSO. Unipolar quantum optoelectronics, including quantum cascade lasers (QCL), Stark modulators, quantum cascade detectors (QCD), and quantum-well IR photodetectors (QWIP), among other components, emerge as potential candidates to build such FSO subsystems and systems. We present our recent efforts in conducting subsystem and system-level studies with different variants of these unipolar quantum optoelectronics and demonstrate the potential for feasible transmitter and receiver performance in a laboratory environment. We also discuss the key challenges and considerations of such technologies towards practical development. Finally, we summarize recent research and development efforts worldwide in advancing this highly promising direction.**

***Index Terms*—free space optics, mid-infrared, unipolar quantum optoelectronics, quantum cascade laser.**

This work was supported in part by the EU H2020 cFLOW Project (828893), in part by the Swedish Research Council (VR) project 2019-05197 and project 'BRAIN' 2022-04798, in part by the LZP FLPP project 'MIR-FAST' lzp 2023-1-0503, and in part by the strategic innovation program Smarter Electronic Systems a joint venture by Vinnova, Formas and the Swedish Energy Agency A FRONTAHUL project (2023-00659) *(Corresponding author: Xiaodan Pang.)*

Mahdieh Joharifar, Richard Schatz, and Yan-Ting Sun are with the Department of Applied Physics, KTH Royal Institute of Technology, 106 91 Stockholm, Sweden (e-mail: mahdieh@kth.se; rschatz@kth.se; yasun@kth.se).

Hamza Dely was with the Laboratoire de Physique de l'École Normale Supérieures, ENS, Université PSL, CNRS, Sorbonne Université, Université de Paris, 75005 Paris, France. He is currently with the Université Paris-Saclay, Paris, France (e-mail: hamza.dely@universite-paris-saclay.fr).

Laureline Durupt was with mirSense, 1 rue Jean Rostand, 91400 Orsay, France. (e-mail: laureline.durupt@gmail.com)

Gregory Maisons is with mirSense, 1 rue Jean Rostand, 91400 Orsay, France (e-mail: gregory.maisons@mirsense.com).

Djamal Gacemi, Angela Vasanelli, and Carlo Sirtori are with the Laboratoire de Physique de l'École Normale Supérieures, ENS, Université PSL, CNRS, Sorbonne Université, Université de Paris, 75005 Paris, France (e-mail: djamal.gacemi@phys.ens.fr; angela.vasanelli@phys.ens.fr; carlo.sirtori@phys.ens.fr).

Lu Zhang and Xianbin Yu are with the College of Information Science and Electronic Engineering, Zhejiang University, Hangzhou 310027, China (e-mail: zhanglu1993@zju.edu.cn; xyu@zju.edu.cn).

Armands Ostrovskis, Toms Salgals, Sandis Spolitis and Vjaceslavs Bobrovs are with the Institute of Photonics, Electronics and Telecommunications, Riga Technical University, 1048 Riga, Latvia (e-mail: armands.ostrovskis@rtu.lv; toms.salgals@rtu.lv sandis.spolitis@rtu.lv; vjaceslavs.bobrovs@rtu.lv).

Oskars Ozolins and Xiaodan Pang are with the Department of Applied Physics, KTH Royal Institute of Technology, 106 91 Stockholm, Sweden, with the RISE Research Institutes of Sweden, 164 40 Kista, Sweden, and also with the Institute of Photonics, Electronics and Telecommunications, Riga Technical University, 1048 Riga, Latvia (e-mail: oskars.ozolins@ri.se; xiaodan@kth.se).

I. Introduction

THE current infrastructure for information and communication technologies (ICT) is primarily limited to terrestrial networks, which consist of fiber-optic and radio access networks. However, the next-generation ICT infrastructure is envisioned to extend beyond terrestrial networks to include multi-altitude layers of networks, spanning all the way from underwater connectivity to air networks and finally to satellite networks [1]. Free-space optical (FSO) communications are becoming an essential part of this paradigm shift process, more than ever, as it extends the capacity and capability of fiber optics into non-terrestrial networks (NTN), e.g., satellite networks and aerial networks. One of the bottlenecks for NTN is identified to be the ground-to-high altitude platforms (HAPs) or ground-to-satellite links. Currently, the most used spectral bands between earth and space are in the radio frequency (RF) range, e.g., the Ku-band (12 to 18 GHz) and the Ka-band (26.5 to 40 GHz) [2]. Following the roadmap of increasing demand for higher data rates, one of the essential targets for practical development of point-to-point FSO systems is to provide robust, reliable communications through long-distance atmospheric channels. This challenge imposed severe concerns on almost all FSO system solutions in the early days, as majority of these systems attempt to reuse mature passive and active optical

This article has been accepted for publication in IEEE/OSA Journal of Lightwave Technology. This is the author's version which has not been fully edited and content may change prior to final publication. Citation information: DOI 10.1109/JLT.2024.3472452

components developed for fiber-optic telecom systems by operating at the short-wave infrared (SWIR, 1-2.5 μm) region. However, SWIR is highly susceptible to atmospheric disturbances like dust, fog, and turbulence effects such as scintillation. These challenges are significantly mitigated by shifting to longer wavelengths [3].

The MWIR (3-5 μm) and LWIR (8-12 μm) bands, two atmospheric transmission windows in the mid-IR region, offer substantial advantages for mid- and long-range outdoor applications [4],[5]. For instance, they provide low propagation attenuation (less than 1 dB/km) and robustness against adverse weather conditions. Specifically, they experience lower Mie scattering from atmospheric particles and are less affected by turbulence-induced scintillation [6]. This makes them ideally suited for practical applications in long-distance atmospheric FSO communications. To exploit these benefits, three main technological approaches have been developed for mid-IR FSO transmissions: the wavelength-conversion approach based on difference frequency generation (DFG) [7]-[13], external modulation based on linear Stark effect [14]-[17], and directly modulated laser sources with either interband cascade lasers (ICLs) [18]-[20], or quantum cascade lasers (QCLs) [21]-[40]. The wavelength-conversion method leverages existing fiber-optic components and multi-dimensional multiplexing schemes to achieve high system data rates and offers great compatibility with fiber-optic telecom systems [41]. Alternatively, semiconductor optoelectronic sources, modulators, and detectors directly operate in the mid-IR, upon maturity, can potentially offer lower energy consumption, smaller footprints, and greater integrability. Recent advances in unipolar quantum optoelectronics (UQOs), including high-bandwidth QCLs, Stark-effect mid-IR modulators, quantum-well IR photodetectors (QWIP) and quantum cascade detectors (QCDs), reassure their potential in the development of mid-IR FSO transceivers.

In this paper, we extend our OFC invited contribution [43] and provide more detailed descriptions, discussions, review and outlook on various aspects of mid-IR FSO communication technologies, with the focus on the recent research and development of UQOs and their applications in FSO systems. The purpose of this work is to provide a comprehensive summary of our progress, offering a clear overview of the current research landscape, and projecting the technological roadmap for the next phase of research. The rest of this article is organized as follows: in Section II, we present the key components, particularly the UQOs that enables our experimental studies of mid-IR FSO transmissions. Section III shows our recent FSO experimental demonstrations empowered by these components, focusing on system-level performance and tradeoffs. In Section IV we discuss the challenges and opportunities of next-step research focuses in driving this technology towards development. Section V summarizes the recent worldwide research and development efforts in relevant directions and extrapolates the technological evolution tendency. Finally, conclusions and an outlook are given in Section VI.

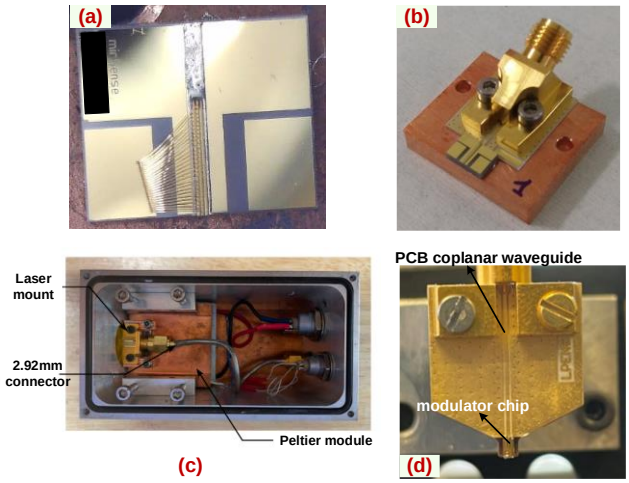

Figure 1. Optoelectronic components for mid-IR FSO transmitters. (a) Picture of a typical QCL submount. (b) QCL module after RF bounding of the submount. (c) Peltier mount hosting the QCL module. (d) Picture of an external Stark modulator operating at 9 μm in the LWIR band.

II. Unipolar Quantum Optoelectronic Components

Unipolar quantum optoelectronics consist of a group of semiconductor devices that can operate in the mid-infrared range with bandwidths on the order of gigahertz. These devices utilize quantum-confined two-dimensional electronic states that form in the conduction band of technologically mature semiconductors. They are referred to as unipolar because only electrons serve as charge carriers in these systems. When selecting components for system-level explorations and demonstrations, we focus on key characteristics such as output power, modulation bandwidth, efficiency, and linearity on the transmitter side, and responsivity, detector bandwidth, and saturation power on the receiver side. It is important to note that devices with these specific characteristics are mostly not commercially available currently, particularly for the LWIR band, due to their low technology readiness level and the limited market size. However, as technology matures and application demand increases, these devices are expected to be developed for practical use. Several key types of UQOs that we have employed in our mid-IR FSO experiments are described in detail as follows.

A. Quantum cascade laser

Quantum cascade lasers, invented in 1994, have seen rapid advancements due to their inherent design potential [44]. They operate based on intersubband transitions within multiple quantum wells (MQW) structures. The design features alternating wells and barriers, typically ranging from 500 to 1000 layers, providing substantial flexibility to innovate with their configurations [45]-[49]. The development of QCLs has significantly benefited from using InGaAs/AlInAs alloys on InP substrates and later GaAs/AlGaAs compositions on GaAs. These materials, which were already well-established due to the advancements in the telecom and photonics industries, provided a robust foundation for the rapid progression of these

new semiconductor lasers. Over time, the evolution of these lasers has increasingly been shaped by the specific demands and requirements of their practical applications, reflecting a shift from theoretical exploration to market-driven development [50]. After the first QCL, researchers have consistently showcased the remarkable versatility enabled by quantum engineering. This includes the development of lasers that emit simultaneously at multiple wavelengths [51], those incorporating integrated sum-frequency nonlinearities [52], and lasers with broadband tunability [53]. The emission properties of these advanced devices stem from modifications made to the quantum-mechanical structure of the active region. Additionally, substantial progress was made in enhancing output power, increasing operating temperatures and enabling continuous-wave (CW) operation through refinements of active region designs [54]-[60].

Single-mode narrow-linewidth tunable mid-IR lasers are crucial for many applications. One predominant method for achieving tunable single-mode operation is distributed feedback (DFB) QCL, with a Bragg grating into the laser waveguide, favoring a single wavelength determined by the grating period [61]. In 2005, a room-temperature CW DFB QCL was demonstrated using a buried grating [62]. To date, continuous improvements have been made in increasing output power, enabling functionality in high temperatures, and reducing power consumption [63]-[69]. Notably, directly modulated (DM)-QCLs feature ultra-short carrier relaxation lifetimes, which enable high intrinsic modulation bandwidths and suppress the resonance frequency by making the laser response over-damped [70]. In recent years, the capability for high bandwidth modulation of QCLs at room temperature has sparked renewed interest in their application in FSO communication [71]. QCLs have been considered for applications in mid-IR and LWIR FSO communications since the early 2000s [21]-[24]. However, progress in this field has fallen behind FSO communications advancements in the 1.55 μm telecom band due to the limited maturity of devices and components operating at these frequencies. Despite this, the evolving requirements for 6G technology create new opportunities for QCLs as additional spectral windows are required for high-speed communications.

Figure 1(a) shows a picture of one of the DFB QCL chips that we employ in our FSO transmission studies. These chips were fabricated by mirSense, and they are designed to operate either in the MWIR or in the LWIR regions. They are engineered to operate in CW mode, delivering several tens of milliwatts of output power. This power level is found sufficient for laboratory FSO communication demonstrations, balancing the need for signal power with thermal management constraints. Figure 1(b) shows a picture of a QCL submount, which houses the QCL laser chip. The RF-bound QCL module, depicted in Figure 2(b), includes a 2.92 mm RF coaxial interface. The connection between the RF interface and the QCL submount is facilitated through a coplanar waveguide on a printed circuit board (PCB). This design ensures minimal signal loss and maintains the integrity of the high-frequency signals required for efficient data transmission. To manage the operational temperature of the QCL, the module is placed in a Peltier mounting module, as shown in Fig. 1(c). The Peltier module is essential for maintaining stable temperature conditions, preventing thermal degradation and ensures optimal operation of the QCL over extended periods.

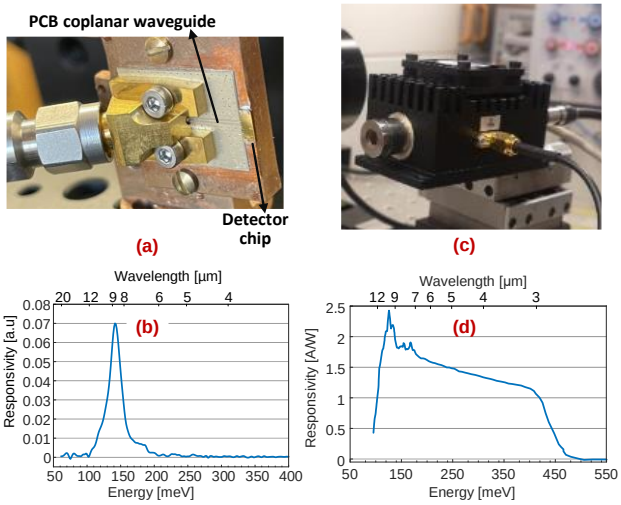

Figure 2. (a) A typical appearance of RF-bounded QCD/QWIP. (b) Responsivity spectrum of the QCD. (c) A commercial MCT detector used for the FSO experiments. (c) Responsivity spectrum of the MCT detector [35],[36].

B. Stark modulator

Similar to optical communications in fiber-optic systems, external amplitude modulators have also been recently designed and developed to perform high-speed modulation in the mid-IR region. The operational principle of this type of modulator is typically based on the intersubband linear quantum Stark effect, achieved by growing asymmetrically doped quantum wells [72],[73]. This effect is the intersubband counterpart of the quantum-confined Stark effect (QCSE), which was originally discovered in interband quantum well structures [74]. Such a design eliminates the need for gate implementation typically required for charge depletion, thereby minimizing intrinsic parasitic capacitances. This approach not only enhances speed but also improves the efficiency and reliability of the device. When operating, by applying alternating electrical field, i.e., the amplitude modulation signal, on the quantum wells, Stark shift of an absorbing optical transition in and out of the laser frequency occurs at the modulator, which in turn modulate the optical signal amplitude propagating through the modulator. This type of Stark modulator can be tuned by applying a DC voltage bias to a certain limit, as the modulation depth would have to be reduced to avoid field breakdown with too large an offset.

Figure 1 (d) shows a semi-packaged Stark modulator that operates at 9 μm. It is an asymmetric quantum well fabricated in the GaInAs/AlInAs platform [75]. The dimension of this modulator is 50 × 50 μm^2, which limits the modulation bandwidth to 8 GHz due to geometric capacitance. Therefore, reducing the dimensions of the modulator can further increase

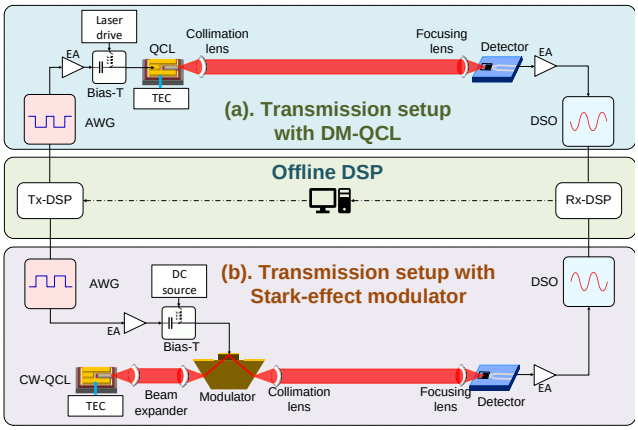

Figure 3. Experimental configurations of mid-IR FSO systems with (a) DM-QCL at the transmitter and (b) external Stark-effect modulator at the transmitter.

the bandwidth. Per simulation, the modulation bandwidth can increase up to almost 20 GHz by reducing the modulator dimensions to 25 × 25 μm^2 [15]. However, this imposes greater challenges of performing accurate light coupling in practical operation, limiting the modulation efficiency and performance.

C. Quantum well infrared photodetector

QWIP was one of the first UQO devices developed for mid-IR applications. In the mid-1980s, its concept and the first QWIP based on GaAs/AlGaAs were reported [76],[77]. QWIP is also based on intersubband transitions within periodically cascaded quantum wells and requires a bias voltage to generate photocurrent. In such a device, a GaAs well with distinct energy levels allows electrons excited by infrared photons to escape into the continuum, and under an applied bias, this results in a net current due to anisotropic electron movement and tunneling from the upper energy level [78]. Typically, a high responsivity level can be reached when operating the QWIP at low temperatures, i.e., below 80 K. However, at room temperature, the performance of QWIP drops drastically by orders of magnitude in terms of responsivity due to enhanced thermal noise. Recently, there have been novel approaches to improve on its performance at room temperature. One proposed method is to insert the heterostructure into a patch antenna resonator array, forming a metamaterial structure [79]. In this way, an antenna effect occurs to significantly enhance the incoming mid-IR electric field and expose it to the heterostructure, thus enhancing the responsivity. Also, by reducing the electrical surface, the capacitance is also reduced, enhancing the bandwidth. High-speed room-temperature mid-IR FSO transmissions can be expected empowered by such a novel detector design that improves on both signal-to-noise ratio (SNR) and bandwidth.

D. Quantum cascade detector

The concept of quantum cascade detector was firstly explored by directly using a QCL as a detector in the early 2000's [80]. Then it was proposed as a new type of QWIP based on electronic tunnelling through the barriers like QCL [81]. Compared with QWIP, QCD has a more complex periodical quantum well structure, which consists of two major parts, i.e., a broad quantum well is located at the beginning of the structure with two highly localized states, then it's followed by a sequence of narrow quantum wells with progressively increasing size, allowing electrons to relax non-radiatively through resonant tunnelling to the next period [82]. Such an intrinsic asymmetrical structure allows the QCD to be operated without any bias voltage. A further improvement was proposed to use first two quantum wells instead of one to create diagonal radiative transition, allowing more efficient electrons extraction, enhancing the detector responsivity [83]. QCDs are also known for their extremely short carrier relaxation times, typically in the picosecond (ps) range [84],[85]. Moreover, QCD generally has small footprint and allows for stable performance without the need for additional cooling modules for room temperature operation. To date, there have been continuous efforts in improving the performance of QCDs in expansive bandwidth, high-temperature operation, and low energy consumption, including embedding the detector in antenna to form a metamaterial pattern [86], like the recent progress in QWIP.

Figure 2(a) displays a LWIR QCD module used in our FSO system experiment, which is analogous to the design reported in [87]. The responsivity spectrum of the QCD is shown in Fig. 2(b). One can observe that the responsivity region of the QCD is concentrated around 9 μm. This localized sensitivity indicates the necessity for designing specific detectors that operate effectively at different wavelengths to match different transmitter lasers.

Besides the UQOs, we also employ mercury cadmium telluride ($Hg_{1-x}Cd_xTe$, MCT) detectors in our mid-IR FSO experiments. In contrast to QCD and QWIP, MCT detector is not a member of UQOs as it is typically based on a bipolar mechanism where both electrons and holes contribute to the charge transport and detection processes [88]. Though with relatively limited bandwidth, MCT detectors are highly sensitive and can operate across a wide spectral range [89]. Figure 2(c) shows an image of a commercial MCT detector module with a built-in transimpedance amplifier (TIA) that we employed in both MWIR and LWIR FSO experiments. The response spectrum of this module, depicted in Fig. 2(d), highlights a wide operational range that spans both transmission windows. This span facilitates the potential use of wavelength-division multiplexing (WDM) configurations with a unified detector design.

III. Transmission System Demonstrations

We have conducted a series of experimental demonstrations using QCLs across both the MWIR and LWIR bands. It is worth noting that, rather than being competing technologies, research efforts in FSO communications in both the MWIR and LWIR bands collectively contribute to building momentum toward achieving viability. As we have reported and summarized our QCL-based MWIR FSO works previously [33],[90], in this paper, we focus on our most recent LWIR FSO system experimental studies. So far, all our

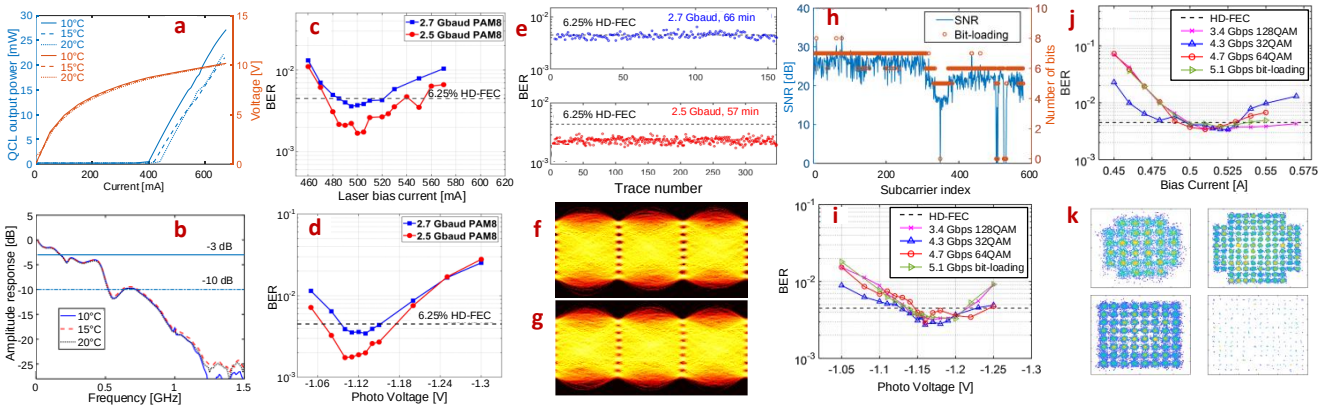

Figure 4 System characteristics and transmission results using a 9.15-μm DM-QCL and the MCT detector of 700 MHz bandwidth with both PAM8 and DMT signal formats. (a) L-I-V curves of the QCL at different temperature values. (b) End-to-end system amplitude response. (c) BER performance versus laser bias current with fixed receiver photovoltage of -1.1 V. (d) BER performance versus receiver photovoltage with fixed laser bias current of 500 mA. (e) System stability test results. Selected eye diagrams of (f) 2.5 Gbaud and (g) 2.7 Gbaud PAM8 signals. (h) The probed SNR values across the SCs and the bit allocation for the SC bit-loading scheme with Chow's algorithm for DMT signal transmissions. (i) BER versus photovoltage with different SC modulations. (j) BER versus laser bias current with different SC modulations. (k) Corresponding subcarrier constellations with different modulation orders after the channel equalization. [35], [38] (IEEE, reprinted with permission.)

experiments have been performed in indoor laboratory environments with short distance between the transmitter and receiver, with the focus on the transceiver subsystems' characteristics and performance.

A. Experimental configuration of FSO transmission systems

Figure 3 depicts experimental configurations of the LWIR FSO transmission systems. Figure 3(a) shows the setup when we use DM-QCL as the transmitter, and Figure 3(b) shows the setup employing an external Stark modulator as transmitters. At the receiving end, we used various types of PDs, including two different MCT detectors and the QCD module described previously.

There are two main strategies to increase the systems' overall bitrates, i.e., first, increasing signal bandwidth, and second, enhancing spectral efficiency. The first strategy involves a comprehensive upgrade of the end-to-end system bandwidth, affecting all bandwidth-limited optical and electrical components and entailing advances in device and material design and fabrication technologies. In contrast, the second strategy utilizes digital pre- and post-equalization techniques alongside FEC codes to attain a BER that meets application requirements [91]. In our experiments, as our systems are mainly bandwidth limited, we adopt both conventional non-return-to-zero on-off keying (NRZ-OOK) and advanced signal formats such as multi-level pulse amplitude modulation (PAM) and discrete multi-tone (DMT) signals. These advanced modulation formats can offer higher spectral efficiencies in bandwidth limited FSO systems, at a cost of higher required SNR [92]. As shown in Fig. 3, signals with various modulation formats were generated as digital samples offline in MATLAB after transmitter-side (Tx) digital signal processing (DSP). These Tx-DSP algorithms include bit-to-symbol mapping and static pre-equalization for PAM, and bit- and power-loading for DMT, after acquiring the channel information. In all our system experiments, we used pseudorandom binary sequences of over one million bit-length, generated using the Mersenne Twister algorithm in MATLAB with a shuffled seed number to ensure stringency. Subsequently, the samples were converted to the analog domain using an arbitrary waveform generator (AWG).

For both direct and external modulation schemes, bias tees were used to deliver the bias current/voltage and modulation signals to the laser/modulator. For the DM-QCL experiments, at the QCL's output, the modulated light beam at the center wavelength of the laser chip was emitted into free space. The beam is first collimated with a collimation lens, which ensures that the beam maintains its integrity and directionality over distances. For the external Stark modulator experiment, to ensure an optimal free-space coupling to the modulator, we needed to firstly expand the beam with a two-lens beam expander setup. In this way we can focus the beam into a small focusing spot to minimize the coupling loss. After modulation, the emitted signal from the modulation is again collimated with a third lens and launched into the free space. After free-space transmission, the beam is gathered using one or two lenses, strategically positioned to accurately focus and direct the light depending on the aperture of the detector. It is noted that the FSO transmission distances vary in different experiments, ranging from 50 cm to 1.5 meters, confined by our optical tabletop size due to lab laser safety regulations.

The received signal is focused onto a detector, generating an electrical output. This output is then amplified and captured using a real-time digital sampling oscilloscope (DSO). The digital samples undergo offline receiver DSP for signal demodulation and bit error rate (BER) counting. For NRZ-OOK and PAM signals, we used data-aided feedforward equalizer (FFE) and the decision-feedback equalizer (DFE). It is worth noting that the AWG and the DSO were connected to the same computer and operated via the same script. This setup created a closed loop that allowed the system to continuously capture and process the received signal in a quasi-real-time manner. This integration facilitated streamlined data handling and analysis, ensuring efficient

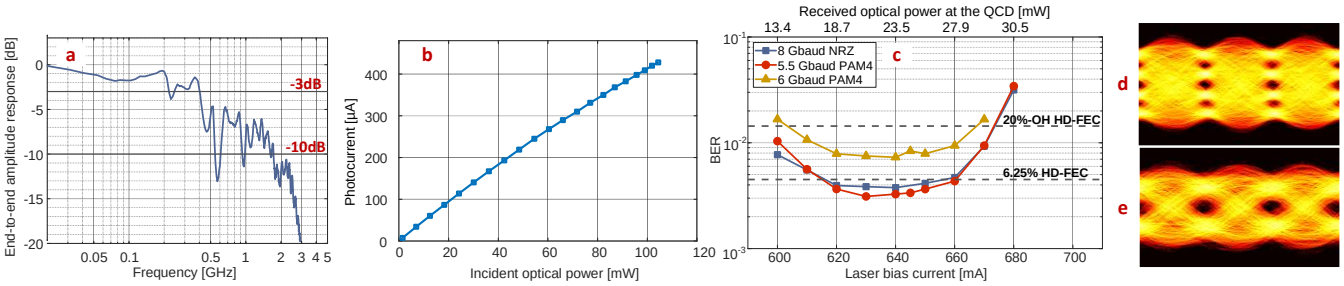

Figure 5 System characteristics and transmission results using a 9.6-μm DM-QCL and the QCD of 2 GHz bandwidth with NRZ-OOK and PAM4 signals. (a) End-to-end system amplitude response when laser operating at 0°C. (b) The measured photocurrent of the uncooled QCD as a function of incident CW optical power. (c) BER as a function of the laser bias current for NRZ-OOK signal at 8 Gbaud and PAM4 signal at 5.5 Gbaud (11 Gb/s) and 6 Gbaud (12 Gb/s). (d). Selected eye diagrams for both the 5.5 Gbaud PAM4 and the 8 Gbaud NRZ-OOK signals measured at optimal laser bias points. [39]

signal processing throughout the experiment.

B. 9-μm FSO using DM-QCL and 700 MHz MCT detector

Figure 4 summarizes our experimental characterizations of an LWIR FSO transmission setup in the LWIR window [37]-[39]. We used a 9.15-μm DM-QCL at the transmitter side, and its light-current-voltage (L-I-V) curves at different temperature are shown in Fig. 4 (a). At the receiver side, we placed a 700 MHz MCT detector. Figure 4(b) shows the end-to-end system bandwidth characterized by generating a frequency comb with the AWG and capturing after modulation and reception with the DSO. As we discussed previously, the MCT detector has superior responsivity and low noise. Therefore, we adopted two spectrally efficient modulation formats, i.e., 8-level PAM (PAM-8) and DMT with this experimental configuration. Figure 4 (c) and (d) shows the BER performances as a function of the transmitter and receiver power, respectively. We observed that there is an optimal laser bias current balancing transmitted power and modulation linearity. Similarly, an optimal received power balancing SNR and detector nonlinearity was also identified. We performed stability tests for PAM-8 signals at two symbol rates, i.e., 2.5 Gbaud and 2.7 Gbaud, and the results are shown in Fig. 4 (e). Stable BER performance was observed in the laboratory environment lasting for about 1 hour. By benchmarking agains the 6.25% overhead (OH) hard-decision forward error correction (HD-FEC) limit [93], the highest achievable gross data rate with PAM-8 in this configuration is 8.1 Gbps. Fig. 4 (f) and (g) shows selected eye diagrams of PAM-8 signals at the two symbol rates, captured at the optimal operational point. Clear eye openings and negligible nonlinear compressions were seen on both diagrams. For DMT, the bit- and power-loading configuration is shown in Fig. 4(h). To explore the highest achievable data rate, similar sweeps on the laser bias current and the received power were performed, as shown in Fig. 4(i) and (j). Figure 4 (k) shows selected subcarrier constellations with different modulation orders. Though through bit- and power-loading the DMT can maximally adapt to the channel response, the time domain signal experienced a very high peak-to-average power ratio (PAPR), limiting the overall SNR across all subcarriers. Consequently, the highest gross data rate achieved with DMT was 5.1 Gbps with this configuration. Therefore, in later experimental studies we focused on PAM modulation formats.

C. 9.6-μm FSO using DM-QCL and QCD

Figure 5 shows the system characterization and transmission performance of a LWIR FSO system using a 9.6-μm DM-QCL at the transmitter and a fully passive QCD at the receiver [39]. This QCL unit has the similar design as the 9.15-μm unit used in previous works. The end-to-end system response is shown in Fig. 5 (a) when operating the laser at 0°C. Figure 5 (b) shows the responsivity characterization of the employed QCD by measuring the generated photocurrent when sweeping the incident optical power. It was observed that only sub-mA photocurrent was generated with tens of mW received optical power, resulting in limited SNR of the received signal. Due to the difficulty of alignment and focusing on the detector side, we only swept the QCL bias current to identify the optimal operation point and kept the received optical power at maximum achievable value. As shown in Fig. 5(c), similar to the previous case, there is an optimal modulation point compromising the tradeoff between power and linearity. With this configuration, the highest achievable gross data rate below the 6.25%-OH HD-FEC limit is 8 Gbps with NRZ-OOK and 11 Gbps with PAM-4. Their eye diagrams are shown in Fig. 5 (e) and (h), respectively. This work was considered a milestone in this research direction, as it achieved over 10 Gbps for the first time with DM-QCL-based LWIR FSO.

D. 9.15-μm FSO using DM-QCL and 1.2 GHz MCT

To further improve the achievable data rate in LWIR FSO, we employed an upgraded commercial MCT photovoltaic detector (ViGO UHSM-10.6) with a bandwidth of 1.2 GHz. Figure 6 (a) shows a picture of the receiver setup. At the transmitter side, we again used the 9.15-μm DM-QCL to benchmark the performance improvement brought in by the new detector [40],[41]. In this round of experiment, we operated the QCL at two temperatures, i.e., 15°C and 20°C and evaluated the transmission performance accordingly. Meanwhile, due to the improved bandwidth compared with the previous MCT detector, we explored lower order modulation formats, namely, NRZ-OOK, PAM-4 and PAM-6, as their SNR requirements are relaxed compared with PAM-8. Figure 6 (b) and (c) shows the BER performance of the three modulation formats at 15°C and 20°C respectively. At 15°C,

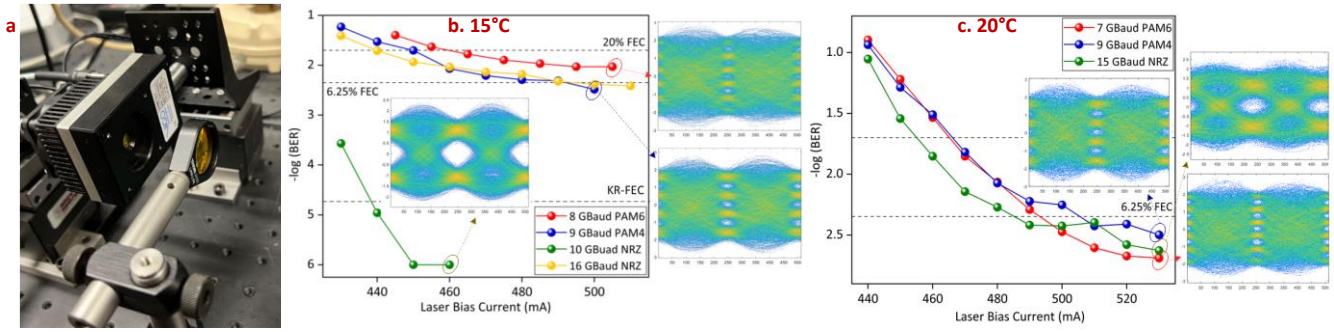

Figure 6 Transmission results using DM-QCL and upgraded MCT detector of 1.2 GHz bandwidth with NRZ-OOK and PAM4 signals. (a) A picture of the receiver configuration with the MCT detector. (b) BER results as a function of laser bias for different modulation formats at 15°C. Insets: Selected eye diagram for 8 GBaud PAM6, 9 GBaud PAM4 and 10 GBaud NRZ. (c) BER results as a function of laser bias for different modulation formats at 20°C. Insets: Selected eye diagram for 7 GBaud PAM6, 9 GBaud PAM4 and 15 GBaud NRZ. [40]

we achieved 16 Gbps NRZ-OOK and 18 Gbps PAM-4 with performance below the 6.25%-OH HD-FEC limit. 8 Gbaud PAM-6 was tested but only achieved BER performance below the 20%-OH SD-FEC limit. A similar performance was achieved at 20°C, with only a slightly lowered NRZ-OOK data rate of 15 Gbps. The eye diagrams for all tested cases are depicted as insets. In summary, a net bit rate of 16.9 Gbps can be achieved PAM4 at both temperatures after deducting the FEC overhead, which is the highest demonstrated LWIR FSO transmission data rate with MCT detectors, to the best of our knowledge.

E. 8.6-μm FSO using Stark modulator and QCD

Finally, we also evaluated the system performance with the external quantum Stark modulator that was previously described in Section II B [16]. In this work, we used a commercial high-power CW QCL as the laser source, which emits up to 80 mW power at a wavelength of 8.6 μm. The emitted beam is firstly expanded then free-space coupled into the quantum Stark modulator through a 60° wedge. Such a design is to increase the coupling length and to facilitate the laser beam alignment [15]. However, a drawback of such a design is that two-thirds of the incident optical power is lost at the facets because of reflections. Therefore, the incident beam to the modulator had to be carefully aligned to minimize the coupling loss. The output modulated LWIR FSO signal from the modulator is again collimated and transmitted over a free-space link before arriving at the receiver. A picture of the modulator configuration setup is shown in Figure 7 (a). To maximally utilize the bandwidth of the modulator, we used the QCD at the receiver. The characterized end-to-end system response is shown in Fig. 7 (b). One can observe that the system presents a mild frequency roll off with around 2 GHz 3-dB bandwidth and a 10 dB cutoff at 7 GHz. After optimization, we kept the setup steady and swept the laser bias current. The BER performances of NRZ-OOK signals at three different data rats are shown in Fig. 7 (c). The highest achieved data rate with this setup was 12 Gbps. It's noted that only 3-tap FFE was used to achieve below HD-FEC limit performance as the system is more noise limited than bandwidth limited. This was validated by sweeping the number of FFE taps from 3 to 55, as shown in Fig. 7 (d). It was observed that the performance improvement by increasing the FFE tap number was marginal. As the system is noise limited, increasing modulation level to higher order PAM didn't provide any improvement on achievable data rate.

IV. Discussions

To date, we have experimentally characterized and evaluated several UQO components and their performance in subsystems and systems for mid-IR FSO communications. We have been focusing on the transmission data rate and the key figure of merits in all our system experiments. However, as all of experimental demonstrations have been carried out in the laboratory environment with short distances between the FSO transmitter and receiver, the main advantages of such UQO devices and the FSO communication system operating in the MWIR and LWIR bands haven't been fully evaluated in real-life scenarios. In the context of mid-IR FSO communications, there is a keen interest in applications spanning considerable distances, often extending to several kilometres for both terrestrial and space applications. Subsequently, there are several critical questions that are yet to be answered.

First, we need to address the challenge of how to achieve sufficient link budget with UQOs-based systems. When transmitting through the atmosphere, the FSO beam degrades due to several factors: 1) beam divergence, which can be analyzed by Gaussian optics; 2) absorption by atmosphere gas molecules; 3) particles-induced scattering; and 4) wavefront deformation due to turbulence [94]. While shifting to longer wavelengths can effectively improve on the latter three factors, it does raise the concern on the pronounced beam divergence compared to shorter wavelengths. A straightforward way forward is to use larger aperture beam expanders at the transmitter side to minimize the divergence. Another possible solution is to adopt large transmitter arrays, similar to the massive multiple-input multiple-output (MIMO) approach in wireless communications, to enable both the transmitter power enhancement and high-directive beamforming.

Second, as we have simply transferred some of the commonly used modulation formats and techniques from fiber-optic communications into our experiments in mid-IR

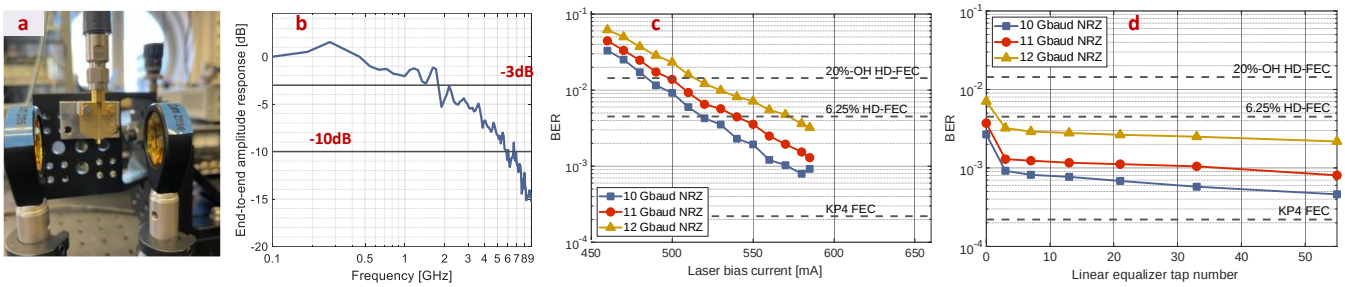

Figure 7 System characteristics and transmission results using the external Stark-effect modulator and the QCD of 2 GHz bandwidth with NRZ-OOK signal. (a) A picture of the modulator operational configuration. (b) End-to-end system amplitude response. (c) BER performance versus laser bias current for three different symbol rates after a 3-tap FFE. (d) BER as a function of the FFE tap number measured at 585 mA laser bias current. [16]

FSO communications, it is yet to be explored the optimal modulation formats that can both effectively address the SNR and bandwidth tradeoff and minimize quality degradation through atmospheric channel propagation. As the mid-IR lies between the RF and SWIR telecom band, tailored modulation formats that combine the merits of both should be identified and systematically analyzed as a future work.

V. Advances in Mid-IR Components and Systems

There have been continuous efforts to improve the performance of components, subsystems and systems on mid-IR FSO communications. On the components level, latest characterisations on the QCL modulation response have demonstrated promising results to support even higher modulation speed than our system demonstrations [95]-[100]. ICLs, which have relatively lower bias current, have also shown inspiring transmission performance in the MWIR band, potentially enabling FSO transceivers with lower power consumption [18]-[20], [101]. Notably, a directly modulated Fabry–Perot ICL at 4.18 μm has been reported to support up to 14 Gbit s^{-1} PAM4 transmission [20]. Moreover, ICLs emitting at LWIR are being designed and developed, with operating temperature approaching thermoelectric cooling range [102],[103]. For external modulators, the next challenge is to realize independent phase and amplitude modulation. A recent work has demonstrated the possibility of utilizing UQOs for phase modulation [104], one step closer to a full coherent modulator at mid-IR region. For detectors, different types of mid-IR detectors have been researched and developed, including QWIP[79],[105]-[107], QCD [108] and uni-traveling carrier photodetector (UTC-PD) [109], continuously improving on detectors' bandwidth and responsivity.

On the system level, Figure 8 provides a comprehensive summary of recent advancements in both the MWIR and LWIR regions, demonstrating transmission rates exceeding 10 Mbps using the three different approaches. The chart in Figure 8(a) tracks the progress of demonstrated single-channel data rates over the years after 2000, highlighting substantial advancements across all three technological strategies over the past decade, particularly over the past 5 years. As we have discussed earlier, the wavelength-conversion approach could already support very high single-channel data rate [7]-[13]. When implementing multi-dimensional multiplexing schemes, this approach has successfully achieved overall system data rates of more than 100 Gbps. Extrapolating from this tendency, one can expect seamless convergence with matched data rate between the fiber optics and mid-IR FSO in the short term with such an approach [41].

With directly modulated laser sources, one of the early studies achieved 100 Mb/s FSO transmission at 3.5-μm in the MWIR band, utilizing a direct-emitting PbCdS diode laser, and its speed was limited by carrier lifetime [110]. Regarding the use of UQOs for mid-IR FSO, several experiments employing a QCL for signal transmission occurred in the early 2000s operating at cryogenic temperatures, supporting up to 2.5 Gbps transmission speed [21]-[24]. During the same period in 2001, Blaser et al. reported the room temperature operation of a 9.3 μm QCL at 258 K, designed to support digital and analog signal transmissions in indoor and outdoor settings [25]. Taslakov et al. published an outdoor transmission over 6000 m using 20 kHz pulse frequency modulation in 2008. This was achieved with a pulsed QCL operated at room temperature [26]. There have been several reports of mid-IR transmissions at room temperature with various signal formats yet performed at relatively low speeds [27]-[29]. Multiple reports after 2010 emerged detailing FSO with terahertz-QCL (THz-QCL) have been reported, although currently, it only supports Mbps scale data rates under cryogenic conditions [111]-[114].

Regarding system demonstrations with external quantum Stark modulators, which potentially provide more sustainable roadmap for high-speed coherent LWIR FSO communications, Didier et al. have recently demonstrated over 20 Gbit s^{-1} FSO transmission at 9 μm using a room-temperature QCD and over 30 Gbit s^{-1} using a nitrogen-cooled QWIP at 77 K [17].

Notably, room-temperature LWIR FSO communications utilizing both external modulators and directly modulated lasers have reached per-channel rates of over 10 Gbps, all within the last two years. Figure 8(b) illustrates the single-channel data rates across different spectral bands, showing a concentration of wavelength-conversion efforts in the MWIR band to optimize conversion efficiency. Furthermore, ICL have shown promising outcomes in the MWIR spectrum. Conversely, the LWIR band primarily features technologies based on external Stark modulator and DM-QCL.

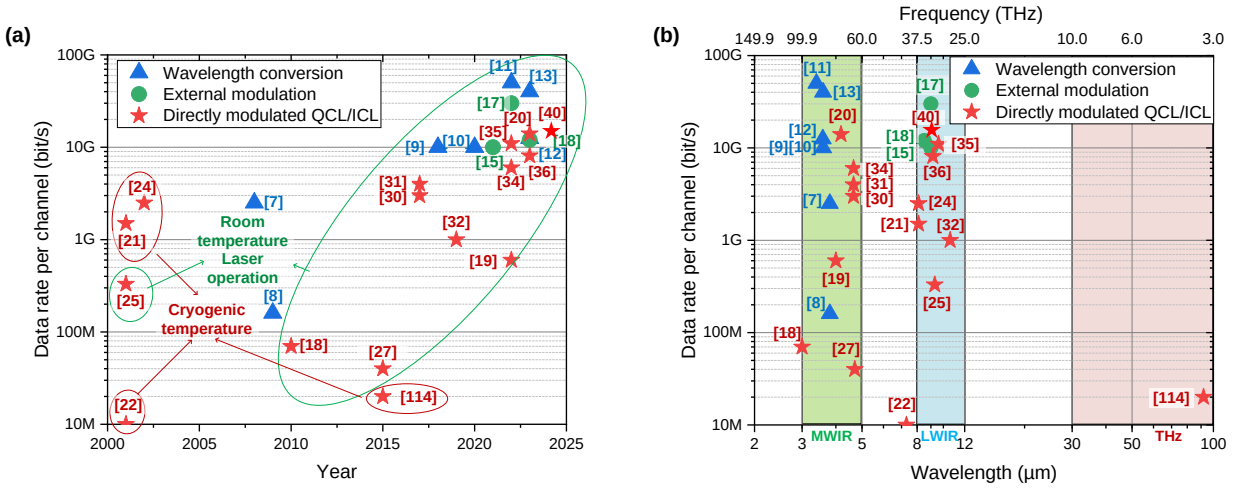

Figure 8. Summary of mid-IR FSO transmission system demonstrations with different schemes, showing (a) the year of publication for each work and (b) the corresponding wavelength/carrier frequency used in each study. Note: This summary is non-exhaustive [7]-[40], [114].

VI. Conclusions and Outlook

We made an overview of the technologies in unipolar quantum optoelectronic devices and their applications in free-space optical communications across the underexploited mid-IR spectral region. We show that novel broadband UQO devices have been continuously developed with improved performance in bandwidth and power, considerably relaxing the FSO system bandwidth limitations. On the other hand, advanced communication system technologies such as modulation, DSP and coding techniques, can maximize the system efficiency and transmission performance with given system bandwidth. There are still many challenges ahead in this area and fundamental research in continuing driving innovations in mid-IR components, subsystems and systems will remain an important task. We also summarized the recent advancements in mid-IR FSO system-level demonstrations with different approaches. Extrapolating from the significant progress over the past few years, one can expect novel technological candidates will converge into viable FSO subsystem- and system-level solutions to fulfill the requirements for future ICT infrastructure.

References

[1] Z. Zhang *et al.*, "6G Wireless Networks: Vision, Requirements, Architecture, and Key Technologies," *IEEE Vehicular Technology Magazine*, vol. 14, no. 3, pp. 28-41, 2019.

[2] O. Kodheli *et al.*, "Satellite Communications in the New Space Era: A Survey and Future Challenges," *IEEE Communications Surveys & Tutorials*, vol. 23, no. 1, pp. 70-109, 2021.

[3] E. Leitgeb *et al.*, "Analysis and evaluation of optimum wavelengths for free-space optical transceivers," in *12th International Conference on Transparent Optical Networks*, 2010, p. Th.B3.1.

[4] L. Flannigan, L. Yoell, and C.-q. Xu, "Mid-wave and long-wave infrared transmitters and detectors for optical satellite communications—a review," *Journal of Optics*, vol. 24, no. 4, p. 043002, 2022.

[5] L. Labadie and O. Wallner, "Mid-infrared guided optics: a perspective for astronomical instruments," *Optics Express*, vol. 17, no. 3, pp. 1947-1962, 2009.

[6] A. Delga, L. Leviandier, M. Razeghi, J. S. Lewis, G. A. Khodaparast, and E. Tournié, "Free-space optical communications with quantum cascade lasers," in *Quantum Sensing and Nano Electronics and Photonics XVI*, 2019, vol. 10926, p. 1092617.

[7] E. Ip *et al.*, "QPSK transmission over free-space link at 3.8 μm using coherent detection with wavelength conversion," in *European Conference on Optical Communication (ECOC)*, 2008, p. Tu.3.E.7.

[8] P. Cho *et al.*, "Optical homodyne RZ-QPSK transmission through wind tunnel at 3.8 and 1.55 micron via wavelength conversion," in *SPIE Defense, Security, and Sensing*, 2009, vol. 7324: SPIE.

[9] Y. Su *et al.*, "10 Gbps DPSK transmission over free-space link in the mid-infrared," *Opt Express*, vol. 26, no. 26, pp. 34515-34528, 2018.

[10] W. Wang *et al.*, "5 Gbaud QPSK coherent transmission in the mid-infrared," *Optics Communications*, vol. 466, 2020.

[11] K. Zou *et al.*, "High-capacity free-space optical communications using wavelength- and mode-division-multiplexing in the mid-infrared region," *Nat Commun*, vol. 13, no. 1, p. 7662, 2022.

[12] Y. Su *et al.*, "150 Gbps multi-wavelength FSO transmission with 25-GHz ITU-T grid in the mid-infrared region," *Optics Express*, vol. 31, no. 9, pp. 15156-15169, 2023.

[13] Y. Su *et al.*, "Free-space transmission of picosecond-level, high-speed optical pulse streams in the 3 μm band," *Optics Express*, vol. 31, no. 17, pp. 27433-27449, 2023.

[14] F. Capasso, C. Sirtori, and A. Y. Cho, "Coupled quantum well semiconductors with giant electric field tunable nonlinear optical properties in the infrared," *IEEE Journal of Quantum Electronics*, vol. 30, no. 5, pp. 1313-1326, 1994.

[15] H. Dely *et al.*, "10 Gbit s−1 Free Space Data Transmission at 9 μm Wavelength With Unipolar Quantum Optoelectronics," *Laser & Photonics Reviews*, vol. 16, no. 2, 2021.

[16] H. Dely *et al.*, "High bitrate data transmission in the 8-14 μm atmospheric window using an external Stark-effect modulator with digital equalization," *Optics Express*, vol. 31, no. 5, 2023.

[17] P. Didier *et al.*, "High-capacity free-space optical link in the midinfrared thermal atmospheric windows using unipolar quantum devices," *Advanced Photonics*, vol. 4, no. 5, p. 056004, 2022.

[18] A. Soibel *et al.*, "Midinfrared Interband Cascade Laser for Free Space Optical Communication," *IEEE Photonics Technology Letters*, vol. 22, no. 2, pp. 121-123, 2010.

[19] O. Spitz *et al.*, "Free-Space Communication With Directly Modulated Mid-Infrared Quantum Cascade Devices," *IEEE Journal of Selected Topics in Quantum Electronics*, vol. 28, no. 1, pp. 1-9, 2022.

[20] P. Didier *et al.*, "Interband cascade technology for energy-efficient mid-infrared free-space communication," *Photonics Research*, vol. 11, no. 4, 2023.

[21] R. Martini *et al.*, "High-speed digital data transmission using mid-infrared quantum cascade lasers," *Electronics Letters*, vol. 37, no. 21, pp. 1290-1292, 2001.

[22] R. Martini *et al.*, "High-speed modulation and free-space optical audio/video transmission using quantum cascade lasers," (in En), *Electronics Letters*, vol. 37, no. 3, pp. 191-193, 2001.

[23] R. Martini *et al.*, "Free-space optical transmission of multimedia satellite data streams using mid-infrared quantum cascade lasers," *Electronics Letters*, vol. 38, no. 4, pp. 181-183, 2002.

[24] F. Capasso et al., "Quantum cascade lasers: Ultrahigh-speed operation, optical wireless communication, narrow linewidth, and far-infrared emission*," IEEE J. Quantum Electron*., vol. 38, no. 6, pp. 511–532, Jun. 2002.

[25] S. Blaser, D. Hofstetter, M. Beck, and J. Faist, "Free-space optical data link using Peltier-cooled quantum cascade laser," *Electronics Letters*, vol. 37, no. 12, pp. 778-780, 2001.

[26] M. Taslakov, S. Mecherle, V. Simeonov, and H. van den Bergh, "Line-of-sight data transmission system based on mid IR quantum cascade laser," in *Free-Space Laser Communication Technologies XX*, 2008, vol. 6877.

[27] C. Liu *et al.*, "Free-space communication based on quantum cascade laser," *Journal of Semiconductors*, vol. 36, no. 9, 2015.

[28] E. Luzhansky, F.-S. Choa, S. Merritt, A. Yu, and M. Krainak, "Mid-IR free-space optical communication with quantum cascade lasers," presented at the Laser Radar Technology and Applications XX; and Atmospheric Propagation XII, 2015, 946512.

[29] E. Luzhansky, F.-S. Choa, S. Merritt, A. Yu, and M. Krainak, "Comparative Analysis of QCL MWIR and SWIR Communication with PPM Signals," in *Imaging and Applied Optics*, 2015, p. JT5A.7.

[30] X. Pang *et al.*, "Gigabit free-space multi-level signal transmission with a mid-infrared quantum cascade laser operating at room temperature," *Optics Letters*, vol. 42, no. 18, pp. 3646-3649, 2017.

[31] X. Pang *et al.*, "4 Gbps PAM-4 and DMT Free Space Transmission using a 4.65-pm Quantum Cascaded Laser at Room Temperature," in *2017 European Conference on Optical Communication (ECOC)*, 2017, p. P2.SC6.31.

[32] J. J. Liu *et al.*, "Mid and long-wave infrared free-space optical communication," in *Laser Communication and Propagation through the Atmosphere and Oceans VIII*, 2019, p. 1113302.

[33] X. Pang *et al.*, "Free-Space Communications Enabled by Quantum Cascade Lasers," *physica status solidi (a)*, vol. 218, no. 3, p. 2000407, 2021.

[34] X. Pang *et al.*, "Direct Modulation and Free-Space Transmissions of up to 6 Gbps Multilevel Signals With a 4.65-µm Quantum Cascade Laser at Room Temperature," *Journal of Lightwave Technology*, vol. 40, no. 8, pp. 2370-2377, 2022.

[35] X. Pang *et al.*, "11 Gb/s LWIR FSO Transmission at 9.6 µm using a Directly-Modulated Quantum Cascade Laser and an Uncooled Quantum Cascade Detector," in *Optical Fiber Communication Conference (OFC) 2022*, p. Th4B.5.

[36] M. Joharifar *et al.*, "8.1 Gbps PAM8 Long-Wave IR FSO Transmission using a 9.15-µm Directly-Modulated QCL with an MCT Detector," in *Optical Fiber Communication Conference (OFC)*, 2023, p. Th1H.1

[37] M. Han *et al.*, "High Spectral Efficiency Long-Wave Infrared Free-Space Optical Transmission With Multilevel Signals," *J. Lightwave Technol.*, vol. 41, no. 20, pp. 6514-6520, 2023.

[38] M. Han *et al.*, "Long-Wave Infrared Discrete Multitone Free-Space Transmission Using a 9.15-µm Quantum Cascade Laser," *IEEE Photonics Technology Letters*, vol. 35, no. 9, pp. 489-492, 2023.

[39] M. Joharifar *et al.*, "High-Speed 9.6-µm Long-Wave Infrared Free-Space Transmission With a Directly-Modulated QCL and a Fully-Passive QCD," *Journal of Lightwave Technology*, vol. 41, no. 4, pp. 1087-1094, 2023.

[40] M. Joharifar *et al.*, "16.9 Gb/s Single-Channel LWIR FSO Data Transmission with Directly Modulated QCL and MCT Detector," in *Optical Fiber Communication Conference (OFC)*, 2024, p. Th2A.25.

[41] M. Joharifar *et al.*, "Advancing LWIR FSO communication through high-speed multilevel signals and directly modulated quantum cascade lasers," *Optics Express*, vol. 32, no. 17, 2024.

[42] A. E. Willner *et al.*, "Free-space mid-IR communications using wavelength and mode division multiplexing," *Optics Communications*, vol. 541, p. 129518, 2023.

[43] X. Pang *et al.*, "Free Space Communication Enabled by Directly Modulated Quantum Cascade Laser," in *Optical Fiber Communication Conference (OFC)*, 2024, p. Th3C.1.

[44] J. Faist, F. Capasso, D. L. Sivco, C. Sirtori, A. L. Hutchinson, and A. Y. Cho, "Quantum Cascade Laser," Science, vol. 264, no. 5158, pp. 553-556, 1994.

[45] Xie, F. *et al.* Room temperature CW operation of short wavelength quantum cascade lasers made of strain balanced Ga*x*In1–*x*As/Al*y*In1–*y*As material on InP substrates. *IEEE J. Sel. Top. Quant.* **17,** 1445–1452 (2011).

[46] B. S. Williams, "Terahertz quantum-cascade lasers," *Nature Photonics*, vol. 1, no. 9, pp. 517-525, 2007.

[47] J. Ulrich, J. Kreuter, W. Schrenk, G. Strasser, and K. Unterrainer, "Long wavelength (15 and 23 µm) GaAs/AlGaAs quantum cascade lasers," *Applied Physics Letters*, vol. 80, no. 20, pp. 3691-3693, 2002.

[48] D. G. Revin, J. P. Commin, S. Y. Zhang, A. B. Krysa, K. Kennedy, and J. W. Cockburn, "InP-Based Midinfrared Quantum Cascade Lasers for Wavelengths Below 4 µm," *IEEE Journal of Selected Topics in Quantum Electronics*, vol. 17, no. 5, pp. 1417-1425, 2011.

[49] J. Faist, F. Capasso, D. L. Sivco, A. L. Hutchinson, S.-N. G. Chu, and A. Y. Cho, "Short wavelength (λ∼3.4 µm) quantum cascade laser based on strained compensated InGaAs/AlInAs," *Applied Physics Letters*, vol. 72, no. 6, pp. 680-682, 1998.

[50] R. F. Curl et al., "Quantum cascade lasers in chemical physics," *Chemical Physics Letters*, vol. 487, no. 1, pp. 1-18, 2010.

[51] A. Tredicucci, C. Gmachl, F. Capasso, D. L. Sivco, A. L. Hutchinson, and A. Y. Cho, "A multiwavelength semiconductor laser," *Nature*, vol. 396, no. 6709, pp. 350-353, 1998.

[52] N. Owschimikow *et al.*, "Resonant Second-Order Nonlinear Optical Processes in Quantum Cascade Lasers," *Physical Review Letters*, vol. 90, no. 4, p. 043902, 2003.

[53] C. Gmachl, D. L. Sivco, R. Colombelli, F. Capasso, and A. Y. Cho, "Ultra-broadband semiconductor laser," *Nature*, vol. 415, no. 6874, pp. 883-887, 2002.

[54] J. Faist *et al.*, "High power mid-infrared (λ∼5 µm) quantum cascade lasers operating above room temperature," *Applied Physics Letters*, vol. 68, no. 26, pp. 3680-3682, 1996.

[55] G. Scamarcio *et al.*, "High-Power Infrared (8-Micrometer Wavelength) Superlattice Lasers," *Science*, vol. 276, no. 5313, pp. 773-776, 1997.

[56] C. Sirtori, J. Faist, F. Capasso, D. L. Sivco, A. L. Hutchinson, and A. Y. Cho, "Mid-infrared (8.5 µm) semiconductor lasers operating at room temperature," *IEEE Photonics Technology Letters*, vol. 9, no. 3, pp. 294-296, 1997.

[57] A. Tredicucci, F. Capasso, C. Gmachl, D. L. Sivco, A. L. Hutchinson, and A. Y. Cho, "High performance interminiband quantum cascade lasers with graded superlattices," *Applied Physics Letters*, vol. 73, no. 15, pp. 2101-2103, 1998.

[58] C. Gmachl *et al.*, "High temperature (T ≥ 425 K) pulsed operation of quantum cascade lasers," *Electronics Letters*, vol. 36, no. 8, pp. 723-725.

[59] J. Faist, M. Beck, T. Aellen, and E. Gini, "Quantum-cascade lasers based on a bound-to-continuum transition," *Applied Physics Letters*, vol. 78, no. 2, pp. 147-149, 2001.

[60] M. Beck et al., "Continuous wave operation of a mid-infrared semiconductor laser at room temperature," *Science*, vol. 295, no. 5553, pp. 301–305, 2002.

[61] Y. Yao, A. J. Hoffman, and C. F. Gmachl, "Mid-infrared quantum cascade lasers," *Nature Photonics*, vol. 6, no. 7, pp. 432-439, 2012.

[62] S. Blaser *et al.*, "Room-temperature, continuous-wave, single-mode quantum-cascade lasers at λ≃5.4µm," *Applied Physics Letters*, vol. 86, no. 4, 2005.

[63] J. S. Yu, S. Slivken, S. R. Darvish, A. Evans, B. Gokden, and M. Razeghi, "High-power, room-temperature, and continuous-wave operation of distributed-feedback quantum-cascade lasers at λ∼4.8µm," *Applied Physics Letters*, vol. 87, no. 4, 2005.

[64] S. R. Darvish, S. Slivken, A. Evans, J. S. Yu, and M. Razeghi, "Room-temperature, high-power, and continuous-wave operation of distributed-feedback quantum-cascade lasers at λ∼9.6µm," *Applied Physics Letters*, vol. 88, no. 20, 2006.

[65] A. Wittmann, Y. Bonetti, M. Fischer, J. Faist, S. Blaser, and E. Gini, "Distributed-Feedback Quantum-Cascade Lasers at 9 µm Operating in Continuous Wave Up to 423 K," *IEEE Photonics Technology Letters*, vol. 21, no. 12, pp. 814-816, 2009.

[66] Y. Bai et al., "Room temperature continuous wave operation of quantum cascade lasers with 12.5% wall plug efficiency," *Appl. Phys. Lett.*, vol. 93, no. 2, 2008, Art. no. 021103.

[67] F. Xie *et al.*, "High-temperature continuous-wave operation of low power consumption single-mode distributed-feedback quantum-cascade lasers at λ∼5.2 µm," *Applied Physics Letters*, vol. 95, no. 9, 2009.

[68] S. Bartalini et al., "Measuring frequency noise and intrinsic linewidth of a room-temperature DFB quantum cascade laser," *Opt. Exp.*, vol. 19, no. 19, pp. 17996–18003, 2011.

[69] J. Zhang *et al.*, " Low-threshold continuous-wave operation of distributed-feedback quantum cascade laser at λ ~ 4.6 μm," *IEEE Photonics Technology Letters*, vol. 23, no. 18, pp. 1334-1336, 2011.

[70] N. Mustafa, L. Pesquera, C. Y. L. Cheung, and K. A. Shore, "Terahertz bandwidth prediction for amplitude modulation response of unipolar intersubband semiconductor lasers," *IEEE Photon. Technol. Lett.*, vol. 11, no. 5, pp. 527–529, May 1999.

[71] M. Carras et al., "Room-temperature continuous-wave metal grating distributed feedback quantum cascade lasers," *Appl. Phys. Lett.*, vol. 96, no. 16, 2010, Art. no. 161105.

[72] J. Teissier *et al.*, "Integrated quantum cascade laser-modulator using vertically coupled cavities," *Applied Physics Letters*, vol. 94, no. 21, 2009.

[73] J. Teissier *et al.*, "Electrical modulation of the complex refractive index in mid-infrared quantum cascade lasers," *Optics Express*, vol. 20, no. 2, pp. 1172-1183, 2012.

[74] D. A. B. Miller *et al.*, "Band-Edge Electroabsorption in Quantum Well Structures: The Quantum-Confined Stark Effect," *Physical Review Letters*, vol. 53, no. 22, pp. 2173-2176, 1984.

[75] C. Sirtori, F. Capasso, D. L. Sivco, A. L. Hutchinson, and A. Y. Cho, "Resonant Stark tuning of second-order susceptibility in coupled quantum wells," *Applied Physics Letters*, vol. 60, no. 2, pp. 151-153, 1992.

[76] L. C. West and S. J. Eglash, "First observation of an extremely large-dipole infrared transition within the conduction band of a GaAs quantum well," *Applied Physics Letters*, vol. 46, no. 12, pp. 1156-1158, 1985.

[77] B. F. Levine, K. K. Choi, C. G. Bethea, J. Walker, and R. J. Malik, "New 10 μm infrared detector using intersubband absorption in resonant tunneling GaAlAs superlattices," *Applied Physics Letters*, vol. 50, no. 16, pp. 1092-1094, 1987.

[78] S. Ehret, H. Schneider, J. Fleissner, P. Koidl, and G. Böhm, "Ultrafast intersubband photocurrent response in quantum-well infrared photodetectors," *Applied Physics Letters*, vol. 71, no. 5, pp. 641-643, 1997.

[79] M. Hakl *et al.*, "Ultrafast Quantum-Well Photodetectors Operating at 10 μm with a Flat Frequency Response up to 70 GHz at Room Temperature," *ACS Photonics*, vol. 8, no. 2, pp. 464-471, 2021.

[80] D. Hofstetter, M. Beck, and J. Faist, "Quantum-cascade-laser structures as photodetectors," *Applied Physics Letters*, vol. 81, no. 15, pp. 2683-2685, 2002.

[81] L. Gendron, M. Carras, A. Huynh, V. Ortiz, C. Koeniguer, and V. Berger, "Quantum cascade photodetector," *Applied Physics Letters*, vol. 85, no. 14, pp. 2824-2826, 2004.

[82] M. Graf, N. Hoyler,M. Giovannini, J. Faist, and D. Hofstetter, "InP-based quantum cascade detectors in the mid-infrared," *Appl. Phys. Lett.*, vol. 88, no. 24, 2006, Art. no. 241118.

[83] P. Reininger *et al.*, "Diagonal-transition quantum cascade detector," *Applied Physics Letters*, vol. 105, no. 9, 2014.

[84] T. Dougakiuchi, A. Ito, M. Hitaka, K. Fujita, and M. Yamanishi, "Ultimate response time in mid-infrared high-speed low-noise quantum cascade detectors," *Applied Physics Letters*, vol. 118, no. 4, 2021.

[85] J. Hillbrand *et al.*, "High-speed quantum cascade detector characterized with a mid-infrared femtosecond oscillator," *Optics Express*, vol. 29, no. 4, pp. 5774-5781, 2021.

[86] G. Quinchard et al., "High speed, antenna-enhanced 10.3 μm quantum cascade detector," *Applied Physics Letters*, vol. 120, no. 9, 2022.

[87] D. Hofstetter, M. Graf, T. Aellen, J. Faist, L. Hvozdara, and S. Blaser, "23GHz operation of a room temperature photovoltaic quantum cascade detector at 5.35μm," *Applied Physics Letters*, vol. 89, no. 6, 2006.

[88] P. Capper and J. Garland, Mercury Cadmium Telluride: Growth, Properties, and Applications (John Wiley & Sons, Ltd, 2011).

[89] W. Lei, J. Antoszewski, and L. Faraone, "Progress, challenges, and opportunities for HgCdTe infrared materials and detectors," *Applied Physics Reviews*, vol. 2, p. 041303, 2015.

[90] X. Pang *et al.*, "Bridging the Terahertz Gap: Photonics-Assisted Free-Space Communications from the Submillimeter-Wave to the Mid-Infrared," *Journal of Lightwave Technology*, vol. 40, no. 10, pp. 3149-3162, 2022.

[91] J. G. Proakis, Digital Communications, Fourth Ed., McGraw-Hill, New York 2001.

[92] X. Pang *et al.*, "Experimental Study of 1.55-μm EML-Based Optical IM/DD PAM-4/8 Short Reach Systems," *IEEE Photon. Technol. Lett.*, vol. 29, no. 6, pp. 523-526, Mar. 2017.

[93] L. M. Zhang, and F. R. Kschischang, "Staircase Codes With 6% to 33% Overhead," J. Lightwave Technol. Vol. 32, no. 10, pp. 1999-2002, 2014.

[94] P. Corrigan, R. Martini, E. A. Whittaker, and C. Bethea, "Quantum cascade lasers and the Kruse model in free space optical communication," *Optics Express*, vol. 17, no. 6, pp. 4355-4359, 2009.

[95] D. Hofstetter, M. Beck, T. Aellen, and S. Blaser, "High-frequency modulation of a quantum-cascade laser using a monolithically integrated intracavity modulator," *IEEE Photonics Technology Letters*, vol. 15, no. 8, pp. 1044-1046, 2003.

[96] A. Hangauer, G. Spinner, M. Nikodem, and G. Wysocki, "High frequency modulation capabilities and quasi single-sideband emission from a quantum cascade laser," *Opt Express*, vol. 22, no. 19, pp. 23439-55, 2014.

[97] B. Hinkov, A. Hugi, M. Beck, and J. Faist, "Rf-modulation of mid-infrared distributed feedback quantum cascade lasers," *Opt Express*, vol. 24, no. 4, pp. 3294-312, 2016.

[98] B. Hinkov et al., "A mid-infrared lab-on-a-chip for dynamic reaction monitoring," *Nat Commun*, vol. 13, no. 1, p. 4753, Aug 13 2022.

[99] K. Yang *et al.*, "Room-temperature quantum cascade laser packaged module at ∼8 μm designed for high-frequency response," *Electronics Letters*, vol. 57, no. 17, pp. 665-667, 2021.

[100] X. Gao *et al.*, "High Frequency Mid-Infrared Quantum Cascade Laser Integrated With Grounded Coplanar Waveguide Transmission Line," *IEEE Electron Device Letters*, vol. 45, no. 4, pp. 649-652, 2024.

[101] O. Graydon, "Interband cascade laser," *Nature Photonics*, vol. 12, no. 10, pp. 568-568, 2018.

[102] J. A. Massengale, Y. Shen, R. Q. Yang, S. D. Hawkins, and J. F. Klem, "Long wavelength interband cascade lasers," *Applied Physics Letters*, vol. 120, no. 9, 2022.

[103] Y. Shen, J. A. Massengale, R. Q. Yang, S. D. Hawkins, and A. J. Muhowski, "Pushing the performance limits of long wavelength interband cascade lasers using innovative quantum well active regions," *Applied Physics Letters*, vol. 123, no. 4, 2023.

[104] H. Dely *et al.*, "Heterodyne coherent detection of phase modulation in a mid-infrared unipolar device," *Optics Express*, vol. 31, no. 19, pp. 30876-30883, 2023.

[105] D. Palaferri *et al.*, "Room-temperature nine-μm-wavelength photodetectors and GHz-frequency heterodyne receivers," *Nature*, vol. 556, no. 7699, pp. 85-88, 2018.

[106] Q. Lin et al., "Real-time, chirped-pulse heterodyne detection at room temperature with 100 GHz 3-dB-bandwidth mid-infrared quantum-well photodetectors," *Optica*, vol. 10, no. 12, 2023.

[107] P. D. Grant, R. Dudek, M. Buchanan, and H. C. Liu, "Room-Temperature Heterodyne Detection up to 110 GHz With a Quantum-Well Infrared Photodetector," *IEEE Photonics Technology Letters*, vol. 18, no. 21, pp. 2218-2220, 2006.

[108] T. Dougakiuchi and N. Akikusa, "Application of High-Speed Quantum Cascade Detectors for Mid-Infrared, Broadband, High-Resolution Spectroscopy," *Sensors*, vol. 21, no. 17, p. 5706, 2021.

[109] J. Huang et al., "High-Speed Mid-Wave Infrared Uni-Traveling Carrier Photodetector Based on InAs/InAsSb Type-II Superlattice," *IEEE Electron Device Letters*, vol. 43, no. 5, pp. 745-748, 2022.

[110] R. Denti, P. A. Andrekson, H. Ahlberg, and S. T. Eng, "3.5 μm optical communication experiment at 100 Mbits−1 using a PbCdS diode laser," *Optical and Quantum Electronics*, vol. 21, no. 1, pp. 69-72, 1989.

[111] Z. Chen *et al.*, "Wireless communication demonstration at 4.1 THz using quantum cascade laser and quantum well photodetector," *Electronics Letters*, vol. 47, no. 17, 2011.

[112] Z. Tan, Z. Chen, J. Cao, and H. Liu, "Wireless terahertz light transmission based on digitally-modulated terahertz quantum-cascade laser," *Chinese Optics Letters*, vol. 11, no. 3, pp. 031403-31405, 2013.

[113] Z. Chen, L. Gu, Z. Tan, C. Wang, and J. Cao, "Real-time video signal transmission over a terahertz communication link," *Chinese Optics Letters*, vol. 11, no. 11, pp. 112001-112003, 2013.

[114] L. Gu, Z. Tan, Q. Wu, C. Wang, and J. Cao, "20 Mbps wireless communication demonstration using terahertz quantum devices," *Chinese Optics Letters*, vol. 13, no. 8, pp. 081402-81404, 2015.